

# Anti-Hawking Phenomena around a Rotating BTZ Black Hole

Matthew P. G. Robbins<sup>1,2,3</sup> and Robert B. Mann<sup>1,2,3,4</sup>

*Department of Physics and Astronomy, University of Waterloo, Waterloo ON, Canada, N2L 3G1  
Perimeter Institute for Theoretical Physics, 31 Caroline Street North, Waterloo ON, Canada, N2L 2Y5  
Waterloo Centre for Astrophysics, University of Waterloo, Waterloo ON, Canada, N2L 3G1 and  
Institute for Quantum Computing, University of Waterloo, Waterloo ON, Canada, N2L 3G1*

In both flat and curved spacetimes, there are weak and strong versions of the anti-Unruh/anti-Hawking effects, in which the KMS field temperature is anti-correlated with the response of a detector and its inferred temperature. We investigate for the first time the effects on the weak and strong anti-Hawking effects for an Unruh-DeWitt detector orbiting a BTZ black hole in the co-rotating frame. We find that rotation can significantly amplify the strength of the weak anti-Hawking effect, whereas it can either amplify or reduce the strength of the strong anti-Hawking effect depending on boundary conditions. For the strong anti-Hawking effect, we find a non-monotonic relationship between the angular momentum and detector temperature for each boundary condition. In addition, we note that the weak anti-Hawking effect is independent of a changing AdS length, while a longer AdS length increases the temperature range of the strong anti-Hawking effect.

## INTRODUCTION

The nature of the quantum vacuum is fundamental to the study of quantum information. By coupling the vacuum field to particle detectors, it is possible to gain understanding of the quantum vacuum and its response to the structure of spacetime. This is particularly interesting if topological features or horizons are present. These detectors are often taken to be simple two-level quantum systems (known as Unruh-DeWitt detectors) that interact with an underlying scalar field, a model that captures the essential features of the light-matter interaction [1, 2]. Such detectors have been employed to study the structure of spacetime [3, 4], black holes [5, 6], and the thermality of de Sitter spacetime [7, 8].

Consider a detector with uniform acceleration in flat spacetime. The detector will experience the Unruh effect, in which the temperature increases in proportion to acceleration [9–11], and heat up. This effect arises because the temperature of the vacuum of one set of modes is different than the vacuum temperature of a second set of modes. Though highly idealized in its original assumptions (such as that of an eternally uniformly accelerating detector), a model-independent derivation of the Unruh effect has been given in the context of axiomatic quantum field theory [12], with the field temperature (given by the Kubo-Martin-Schwinger (KMS) condition [13–15]) and the temperature measured by the detector being the same. There have since been many demonstrations that detectors undergoing other forms of acceleration (non-uniform, circular) get hot [16–22]. In these more general situations the field temperature is positively correlated with the detector temperature, with the latter a monotonically increasing function of the former.

In the last few years it has been shown that some physical situations exhibit the so-called *anti*-Unruh effect instead, in which the temperature of the field is no longer positively correlated with that measured by the

detector [23, 24]. This anti-Unruh effect can be split into two cases: a weak Anti-Unruh effect (as the temperature of the field increases, the detector clicks less often) and a strong Anti-Unruh effect (the field temperature and detector temperature are inversely related) [24].

When considering black holes, the Hawking effect is the analogue of the Unruh effect [25]. While in general detector temperatures are positively correlated with the field temperature outside a black hole [26–29], recently an anti-Hawking effect was shown to also exist, in which a static Unruh-DeWitt (UdW) detector exhibited both strong and weak versions of the phenomenon [30]. This was explicitly demonstrated for the (2+1) dimensional static Banados-Teitelboim-Zanelli (BTZ) black hole. For sufficiently small black holes, the temperature measured by the detector would decrease as the Kubo-Martin-Schwinger (KMS) field temperature of the Hawking radiation increased. The anti-Hawking effect has since been observed for a broader range of boundary conditions [31], though its weak version is not observed for massless topological black holes in four spacetime dimensions [32].

The effects of spacetime dragging due to rotation on these phenomena are much less understood. The quantum vacuum around a rotating black hole is known to exhibit features significantly different from its non-rotating counterpart [33–35]. Several investigations of the behaviour of quantum scalar fields in the background of a rotating BTZ black hole have been carried out [36–39], and studies investigating the response of Unruh-DeWitt detectors in such spacetimes have also been undertaken [26]. Recently it was shown that rotation has very significant effects on the entanglement harvesting abilities of UdW detectors, with the harvested entanglement being considerably amplified at intermediate distances (about 20-50 horizon radii) from the black hole [40].

Motivated by this, we study here the implications of rotation for the anti-Hawking effect. We find that rotation increases the intensity of the weak anti-Hawking effect, but has a negligible influence on its threshold crit-

ical temperature. However for the strong anti-Hawking effect, we find that there is a strong dependence on the angular momenta, with the effect becoming stronger or weaker depending on the boundary conditions. The influence of AdS length on the strong and weak versions of the effect is likewise distinct: the weak anti-Hawking effect is independent of AdS length whereas the strong version sees an increased temperature range.

## UNRUH-DEWITT DETECTORS

To model the interaction between the detectors and the field, we take the detectors to be two-level quantum systems with ground state  $|0\rangle_D$  and excited state  $|1\rangle_D$ , separated by an energy gap  $\Omega_D$ . We shall assume that these detectors have a spacetime trajectory  $x_D(\tau)$ . The interaction Hamiltonian is

$$H_D = \lambda \chi_D(\tau) (e^{i\Omega_D \tau} \sigma^+ + e^{-i\Omega_D \tau} \sigma^-) \otimes \phi[x_D(\tau)], \quad (1)$$

where the switching function dictating the duration of the interaction between the detector and field is  $\chi_D(\tau)$ .  $\lambda \ll 1$  is the field-detector coupling constant, and the ladder operators that raise and lower the energy levels of the detectors are  $\sigma^+ = |1\rangle_D \langle 0|_D$ ,  $\sigma^- = |0\rangle_D \langle 1|_D$ , respectively.

Let the initial state of the detector-field system be  $|\Psi_i\rangle = |0\rangle_D |0\rangle$ . The final state after a time  $t$  is then  $|\Psi_f\rangle = U(t, 0) |\Psi_i\rangle$ , where  $U(t, 0) = \mathcal{T} e^{-i \int dt [\frac{d\tau_D}{dt} H_D(\tau_D)]}$ , with  $\mathcal{T}$  being the time-ordering operator. With the reduced density operator  $\rho = \text{Tr}_\phi |\Psi_f\rangle \langle \Psi_f|$  being the state of the system after integrating over the field's degrees of freedom, we have [3, 41]

$$\rho_{AB} = \begin{pmatrix} 1 - P_D & 0 \\ 0 & P_D \end{pmatrix} + \mathcal{O}(\lambda^4), \quad (2)$$

where

$$P_D = \lambda^2 \int d\tau_D d\tau'_D \chi_D(\tau_D) \chi_D(\tau'_D) e^{-i\Omega_D(\tau_D - \tau'_D)} W(x_D(\tau_D), x_D(\tau'_D)) \quad (3)$$

is the detector's transition probability. We note that this quantity depends on the two-point correlation function,  $W(x, x') = \langle 0 | \phi(x) \phi(x') | 0 \rangle$  (also called the Wightman function) of the vacuum. From the transition probability, we can then define the response function,

$$\mathcal{F} = \frac{P_D}{\lambda^2 \sigma}, \quad (4)$$

where  $\sigma$  describes the timescale of interaction between the field and the detector. In this paper, we shall focus on a Gaussian switching function,  $\chi_D(\tau) = e^{-\frac{\tau^2}{2\sigma^2}}$ .

We will consider fields whose Wightman functions obey the relation

$$W(\tau - i/T_{KMS}, \tau') = W(\tau', \tau) \quad (5)$$

known as the Kubo-Martin-Schwinger (KMS) condition [13–15]. The quantity  $T_{KMS}$  in (5) can be regarded as the temperature of the quantum field in the spacetime. It depends only on the nature of the quantum field and the spacetime background.

Correspondingly, we can also define the detector's temperature from its excitation to de-excitation ratio (EDR). Let

$$\mathcal{R} = \frac{\mathcal{F}(\Omega)}{\mathcal{F}(-\Omega)}, \quad (6)$$

such that there exists a temperature,  $T$ , that obeys the same form of the KMS condition [42],

$$\mathcal{R} = e^{-\Omega/T}. \quad (7)$$

Labelling the temperature that obeys this condition by  $T_{EDR}$ , we have

$$T_{EDR} = -\frac{\Omega}{\log \mathcal{R}} \quad (8)$$

The quantity  $T_{EDR}$  can be regarded as the temperature that the UdW detector registers in the spacetime.

Normally we expect  $T_{EDR}$  and  $T_{KMS}$  to be positively correlated: as the black hole gets hotter, the field temperature increases and the temperature registered by the UdW detector likewise increases. This is indeed the case for most situations in black hole physics. As noted above, it was recently shown that this is not always the case [30], and that sometimes the contrary situation, known as the anti-Hawking effect, occurs. As with the anti-Unruh effect [23, 24], we define

$$\frac{d\mathcal{F}(\Omega)}{dT_{KMS}} < 0 \quad \text{weak} \quad (9)$$

$$\frac{\partial T_{EDR}}{\partial T_{KMS}} < 0 \quad \text{strong} \quad (10)$$

for the weak and strong anti-Hawking effects respectively.

## ROTATING BTZ BLACK HOLES

We can write the action of our system as  $S = S_{EH} + S_\phi$ , where

$$S_{EH} = \frac{1}{16\pi} \int R \sqrt{-g} d^3x \quad (11)$$

is the Einstein-Hilbert action ( $R$  is the Ricci scalar and  $g$  is the determinant of the metric tensor  $g_{\mu\nu}$ ) and

$$S_\phi = - \int \left( \frac{1}{2} g^{\mu\nu} \partial_\mu \phi \partial_\nu \phi + \frac{1}{16} R \phi^2 \right) \sqrt{-g} d^3x \quad (12)$$

is the action for a conformally-coupled scalar field  $\phi$ . We are interested in analyzing both the KMS temperature of the field and the EDR temperature of a detector near a rotating BTZ black hole, whose line element is [43]

$$ds^2 = -(N^\perp)^2 dt^2 + f^{-2} dr^2 + r^2 (d\phi + N^\phi dt)^2 \quad (13)$$

where,  $N^\perp = f = \sqrt{-M + \frac{r^2}{\ell^2} + \frac{J^2}{4r^2}}$  and  $N^\phi = -\frac{J}{2r^2}$  with  $M = \frac{r_+^2 + r_-^2}{\ell^2}$  the mass of the black hole and  $J =$

$\frac{2r_+ r_-}{\ell}$  its angular momentum. The Hawking temperature is

$$T_H = \frac{1}{2\pi\ell} \left( \frac{r_+^2 - r_-^2}{r_+} \right), \quad (14)$$

where the inner and outer horizon radii are denoted by  $r_-$  and  $r_+$ , and  $\ell$  is the AdS length. Note that  $|J| \leq M\ell$ , with extremality occurring when  $r_+ = r_-$  (i.e.  $J = M\ell$ ).

In the Hartle-Hawking vacuum, a conformally coupled-scalar field has a Wightman function that can be written as the image sum over the Wightman functions for AdS<sub>3</sub> [44, 45],

$$W_{BTZ}(x, x') = \sum_{n=-\infty}^{\infty} \eta^n W_{AdS_3}(x, \Gamma^n x') \quad (15)$$

where  $\Gamma x'$  takes  $(t, r, \phi) \rightarrow (t, r, \phi + 2\pi)$ ,  $\eta = 1$  is an untwisted scalar field and  $\eta = -1$  is a twisted scalar field. This yields [26, 27]

$$W_{BTZ} = \frac{1}{4\pi} \frac{1}{2\sqrt{\ell}} \sum_{n=-\infty}^{\infty} \eta^n \left( \frac{1}{\sqrt{\sigma_\epsilon(x, \Gamma^n x')}} - \frac{\zeta}{\sqrt{\sigma_\epsilon(x, \Gamma^n x') + 2}} \right) \quad (16)$$

where

$$\begin{aligned} \sigma_\epsilon(x, \Gamma^n x')^2 = & -1 + \sqrt{\alpha(r)\alpha(r')} \cosh \left[ \frac{r_+}{\ell} (\Delta\phi - 2\pi n) - \frac{r_-}{\ell^2} (t - t') \right] \\ & - \sqrt{(\alpha(r) - 1)(\alpha(r') - 1)} \cosh \left[ \frac{r_+}{\ell^2} (t - t') - \frac{r_-}{\ell} (\Delta\phi - 2\pi n) \right] \end{aligned} \quad (17)$$

and

$$\alpha(r) = \frac{r^2 - r_-^2}{r_+^2 - r_-^2} \quad \Delta\phi = \phi - \phi' \quad (18)$$

with the respective boundary conditions as  $\zeta = 1$  (Dirichlet),  $\zeta = 0$  (transparent), and  $\zeta = -1$  (Neumann). We shall take the detector to have switching function  $\chi_D(\tau_D) = e^{-\tau_D^2/2\sigma^2}$  and only consider untwisted scalar fields with  $\eta = 1$ .

To calculate the transition probabilities, we will work in the co-rotating frame of the detectors [26]:

$$t = \frac{\ell r_+ \tau}{\sqrt{r^2 - r_+^2} \sqrt{r_+^2 - r_-^2}} \quad (19)$$

$$\phi = \frac{r_- \tau}{\sqrt{r^2 - r_+^2} \sqrt{r_+^2 - r_-^2}}. \quad (20)$$

in which case [46]

$$T_{KMS} = T_H / \gamma, \quad (21)$$

where

$$\gamma = \frac{\sqrt{r^2 - r_+^2} \sqrt{r_+^2 - r_-^2}}{r_+} \quad (22)$$

is the Lorentz factor. Straightforward calculations show that we can rewrite equation (3) as  $P_D = \sum_{n=-\infty}^{\infty} \eta^n \{I_n^- - \zeta I_n^+\}$ , where

$$I_n^\pm = K_P \int_{-\infty}^{\infty} dz \frac{e^{-a(z - \frac{2\pi n r_-}{\ell})^2} e^{-i\beta(z - \frac{2\pi n r_-}{\ell})}}{\sqrt{(\cosh(\alpha_n^\pm) - \cosh(z))}} \quad (23)$$

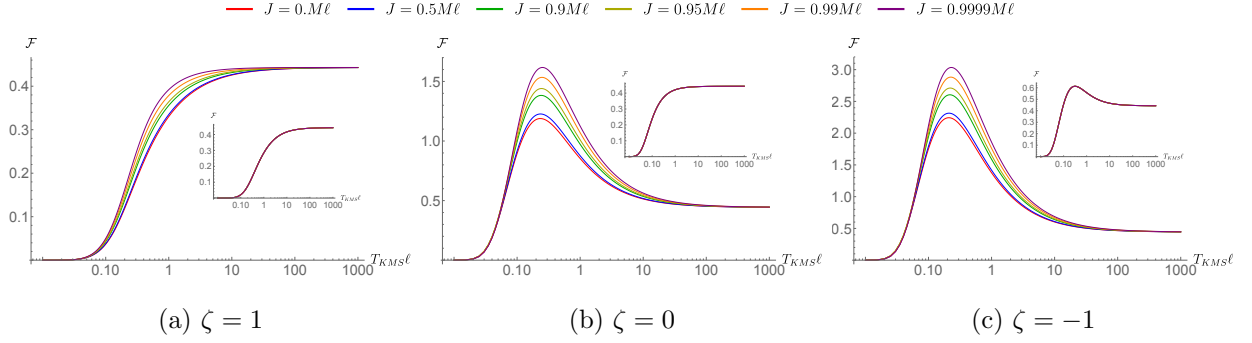


FIG. 1: Response functions for a black hole of mass  $M = 1/10$  for Dirichlet, transparent, and Neumann boundary conditions and an energy gap of  $\Omega\ell = 1/10$ . The inset plots correspond to  $M = 100$ . As expected, the rotation of the black hole has a smaller effect for larger masses. As the mass of the black hole increases, the weak anti-Hawking effect goes away for  $\zeta = 1$  and  $\zeta = 0$ . Note that for  $\zeta = -1$ , the weak anti-Hawking effect is still present even for large mass black holes, with the distinctions between the different rotation parameters so tiny that the curves effectively all overlap.

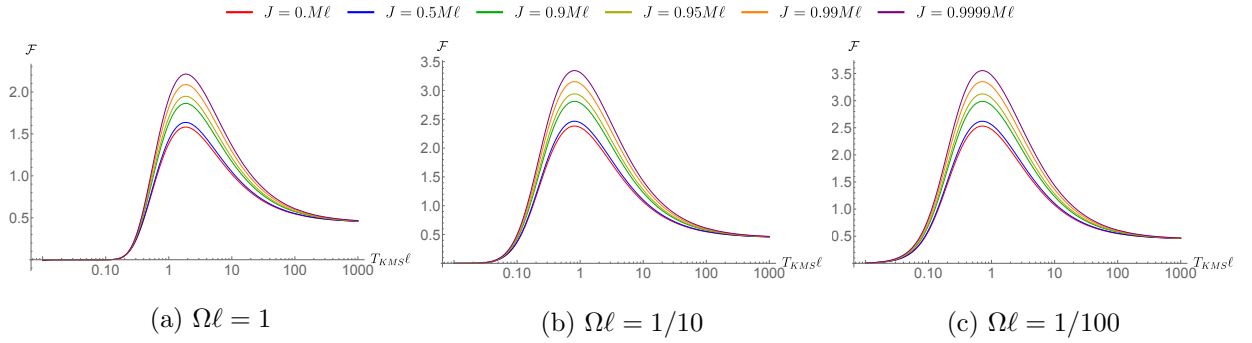


FIG. 2: Response of a rotating BTZ black hole with mass  $M = 1/1000$  and Dirichlet boundary conditions ( $\zeta = 1$ ). We note that for transparent and Neumann boundary conditions, qualitatively similar results are obtained.

and

$$K_P = \frac{\lambda^2 \sigma_D}{4\sqrt{2\pi}} \quad (24)$$

$$a = \frac{1}{(4\pi T_{KMS} \sigma_D)^2} \quad \beta = \frac{\Omega_D}{2\pi T_{KMS}} \quad (25)$$

$$\cosh(\alpha_n^\pm) = \pm 4\ell^2 \pi^2 T_{KMS}^2 + (1 + 4\ell^2 \pi^2 T_{KMS}^2) \cosh \frac{2\pi n r_+}{\ell} \quad (26)$$

In the limit of an infinite interaction time (i.e.  $\sigma \rightarrow \infty$ ), we note that we can write the  $n = 0$  term (corresponding to AdS spacetime) analytically as

$$\lim_{\sigma \rightarrow \infty} P_{D,n=0} = \lim_{\sigma \rightarrow \infty} I_0 = \frac{\sqrt{\pi}}{4} \left[ 1 - \tanh \frac{\Omega_D}{2T_{KMS}} \right] [1 - \zeta P_{-1/2+i\beta}(\cosh \alpha_0^+)] \quad (27)$$

To investigate the influence of rotation (and AdS length) on the weak and strong anti-Hawking effects, we must determine the dependence of the response function and EDR temperature on the KMS temperature. To vary the latter, we locate the detector at  $r = R_D$  in the co-rotating frame and solve (21) and (22) for  $R_D$  in

terms of  $T_{KMS}$  and the other parameters. The response  $P_D$  in (3) and the EDR temperature are then functions of  $T_{KMS}$ .

## WEAK ANTI-HAWKING EFFECT FOR ROTATING BTZ BLACK HOLES

To set the context for our investigation, we first compare the situation for large and intermediate mass black holes with a detector energy gap of  $\Omega_D \ell = 1/10$  (with other energy gaps yielding qualitatively similar results). This is shown in Figure 1, where we plot detector response as a function of  $T_{KMS}$ . The general trend is that for both masses and all boundary conditions the response is suppressed at small KMS temperatures and asymptotes to a constant value at a large ones. Apart from these two general features, there is notably distinct behaviour as these parameters are varied. In the main figure, we depict the situation for an intermediate mass  $M = 1/10$ , where we see that rotation has marginal impact at small and large KMS temperatures, but significantly amplifies detector response at intermediate KMS temperatures. An even larger influence is due to boundary conditions, where we observe that the weak anti-Hawking effect is absent for Dirichlet boundary conditions, but present for the other two. The negative slope to the right of the peak is steeper for Neumann boundary conditions, indicative of increasing strength of the weak effect as  $\zeta$  decreases. In the inset of each subfigure, we consider the large mass  $M = 100$  case, where we see that the weak anti-Hawking effect disappears for  $\zeta = 1, 0$  boundary conditions, yet remains for  $\zeta = -1$ , recovering earlier results [30] for large-mass black holes. We see that there is negligible dependence of the response on angular momentum in this large mass case for all KMS temperatures.

It is clear from this that rotational effects are more pronounced for smaller mass black holes, and so in Figure 2, we plot the dependence of the response function on KMS temperature for  $M = 1/1000$ . The weak effect is now clearly evident for Dirichlet boundary conditions, with the peak response enhanced as much as sevenfold, compared to the left diagram in Figure 1. Similar results hold for the other boundary conditions. As before, as rotation increases, the response is amplified for all values of  $T_{KMS}$ . For all values of rotation and all gaps, the response asymptotes to a value of  $P_D = \frac{\sqrt{\pi}}{4}$ , in accord with equation (27), noting from equation (23) that  $I_n \rightarrow 0$  for  $n \neq 0$ .

The strength of the weak anti-Hawking effect depends on the magnitude of the negative value of the slope of equation (9) after the peak. We see that this increases with decreasing gap, showing that smaller gap enhances the weak anti-Hawking effect, which we illustrate for Dirichlet boundary conditions in Figure 3. The slope peaks at  $\frac{d\mathcal{F}}{dT_{KMS}\ell} \approx -0.15$  for the large energy gap and  $\frac{d\mathcal{F}}{dT_{KMS}\ell} \approx -0.6$  for the small gap. For each gap, we also see that the weak anti-Hawking effect is amplified with increasing rotation, by as much as 50% for near-extremal black holes, for all gaps in the figure.

Furthermore, we find that the weak anti-Hawking ef-

fect occurs after a critical value of  $T_{KMS}$  that depends on the detector's energy gap, but not on the rotation of the black hole, again evident from Figure 3. Though we have only illustrated results for Dirichlet boundary conditions  $\zeta = 1$ , we emphasize that this critical value depends on  $\zeta$ , with the critical temperature becoming smaller as  $\zeta \rightarrow 1$ .

Finally, we note that changing the AdS length will not change the strength of the weak effect. Physically, this is because the AdS length is the only length scale present (as  $\sigma \rightarrow \infty$ ), and everything is calibrated against this length.

## STRONG ANTI-HAWKING EFFECT FOR ROTATING BTZ BLACK HOLES

Let us now turn our attention to the strong anti-Hawking effect. In Figures 4 and 5, we plot the relationship between the EDR and KMS temperatures for  $M = 1/1000$  and different boundary conditions, with  $\Omega\sigma = 1$  and  $\Omega\sigma = 1/10$ , respectively. We note several interesting features.

First, it is evident from Figure 4 that a strong anti-Hawking effect is present for all three boundary conditions. This is clear at low values of  $T_{KMS}$ , where we see a negative slope indicative of the strong effect. Eventually a minimum is reached and  $T_{EDR}$  begins to increase with  $T_{KMS}$ . The insets indicate the behaviour at large  $T_{KMS}$ , where we see that this quantity is indeed positively correlated with  $T_{EDR}$ , and there is minimal dependence on angular momentum, even for small  $M$ . Unlike the weak effect, we see that the maximum decreases with increasing values of angular momentum for all boundary conditions. Consequently the strength of the strong effect (the slope in equation (10)) likewise diminishes. As extremality is approached, the strong effect essentially vanishes.

The exception is for Dirichlet boundary conditions. In Figure 5, we plot the EDR temperature for Dirichlet boundary conditions for  $\Omega\sigma = 1$  and  $\Omega\sigma = 1/100$ . In the insets, we see that there is a small strong anti-Hawking effect for non-rotating black holes, similar to what was found in [30]. As the angular momentum increases, the peak in Figure 5 moves rightward, and the threshold value of  $T_{KMS}$  at which the strong effect appears increases. This threshold value will reach a maximum for some  $J/M\ell$ , after which it decreases with increasing  $J/M\ell$  as extremality is approached, as is clear from Figure 6. We also qualitatively see that the magnitude of the slope becomes larger for larger angular momenta, indicating that the strong anti-Hawking effect becomes stronger. For smaller values of the energy gap, we see that the strong anti-Hawking effect increases in strength, with the  $\Omega\sigma = 1/10$  case being similar to  $\Omega\sigma = 1/100$ . This can be seen by noting that  $J/M\ell = 0.9$  does not exhibit the strong anti-Hawking effect for  $\Omega\sigma = 1$ , but

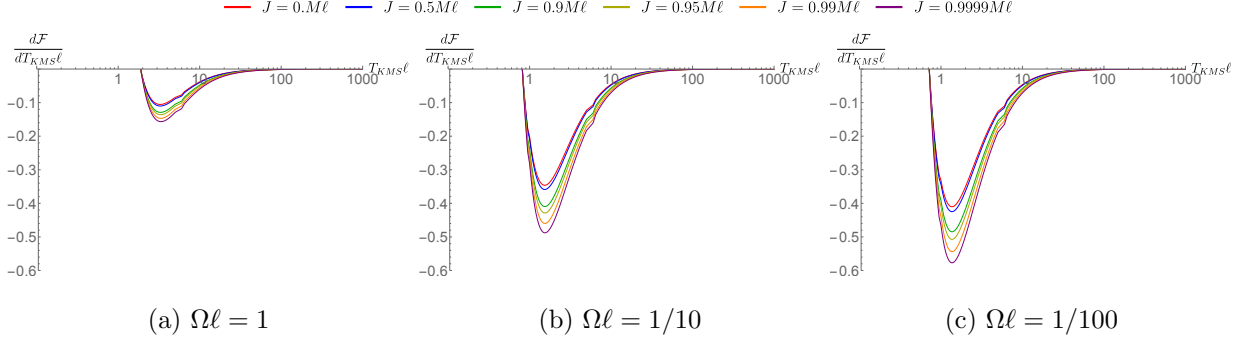


FIG. 3: Derivative of the response with respect to the KMS temperature (9) of a rotating BTZ black hole with mass  $M = 1/1000$ , and Dirichlet boundary conditions ( $\zeta = 1$ ). We note that for transparent and Neumann boundary conditions, qualitatively similar results are obtained.

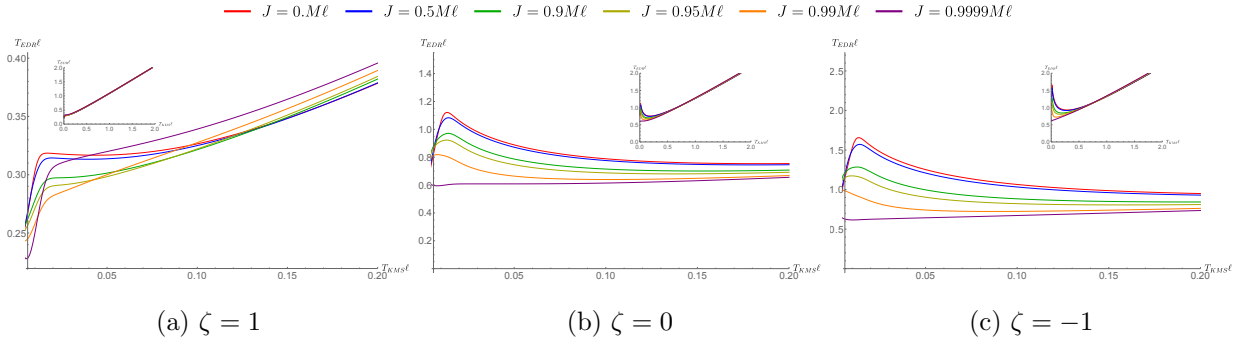


FIG. 4: EDR temperature for a black hole of mass  $M = 1/1000$  and energy gap of  $\Omega\sigma = 1$ . We plot KMS temperature down to  $T_{KMS}l = 10^{-5}$ . The insets show the relation between the EDR temperature and KMS temperature for larger values of  $T_{KMS}$ .

there is a small effect present at this value of the angular momentum for  $\Omega\sigma = 1/100$ .

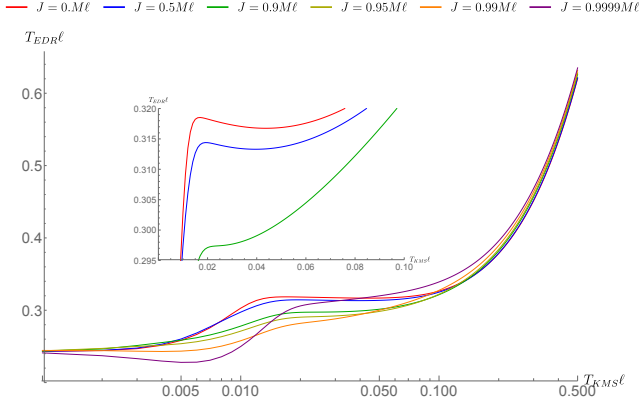
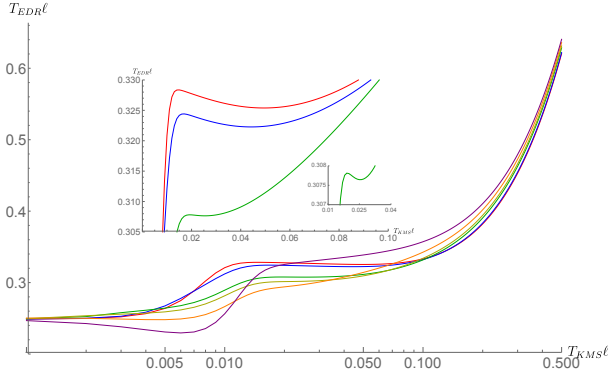
For transparent and Neumann boundary conditions, we find that the strong anti-Hawking effect is much more pronounced, as can be seen from Figure 4. Furthermore, as  $\zeta$  increases from  $-1$  to  $1$  in Figure 4, the range of  $T_{KMS}l$  over which the strong effect is present also decreases, and is very small for Dirichlet boundary conditions. This range decreases with increasing angular momentum for transparent and Neumann boundary conditions. There is a minimal value of  $T_{EDR}l$  as function of  $T_{KMS}l$ , and this minimal value decreases as the angular momentum of the black hole increases.

For Dirichlet boundary conditions and sufficiently small angular momentum, larger angular momenta also yields a decreasing range of  $T_{KMS}$  temperatures for which the strong effect holds, up to a critical value of  $J/Ml$ . Beyond this value, increasing angular momenta results in a greater range of  $T_{KMS}$  temperatures for which the effect is present. As a result, the anti-Hawking effect appears to nearly disappear for near-extremal black holes  $J \geq 0.9999Ml$  for transparent and Neumann boundary conditions, yet is still present for Dirichlet boundary conditions. In Figure 5, we see that

there is a strong anti-Hawking effect for a non-rotating black hole, but the effect disappears (or almost disappears, depending on the energy gap) as the angular momentum increases to  $J/Ml = 0.9$ .

Beyond this, however, as we continue to approach extremality in the Dirichlet case, the strong effect emerges at lower KMS temperatures, as shown in Figure 6. Indeed, its range and strength both get larger as  $J/Ml$  gets very close to unity, as evidenced by the curve for  $J/Ml = 0.9999$ . It is quite remarkable that there is such a strong dependence on boundary conditions.

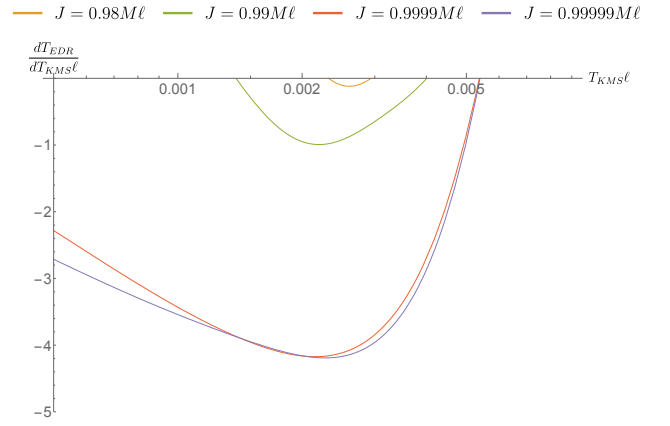
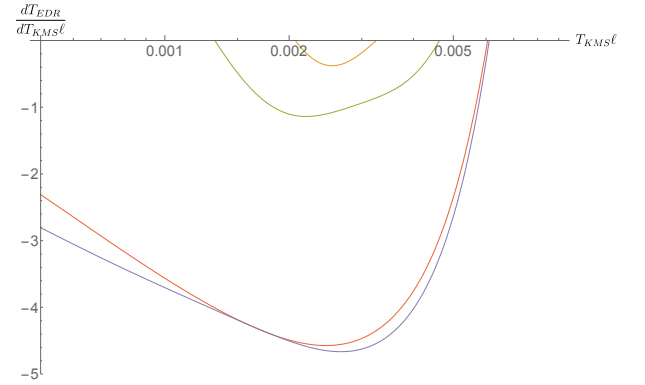
Finally, inspection of Figures 4 and 5 indicate that the strong effect does not monotonically depend on  $J/Ml$ . Indeed, we observe a ‘crossover’ effect at small  $T_{KMS}$ , in which the values of  $T_{EDR}$  decrease with increasing angular momentum as  $T_{KMS} \rightarrow 0$ , whereas at sufficiently large  $T_{KMS}$  the rate of change of  $T_{EDR}$  with respect to  $T_{KMS}$  increases with increasing angular momentum such that the higher- $J$  curves cross over the lower- $J$  curves. At large  $T_{KMS}$ , we see that  $T_{EDR} \sim T_{KMS}$ , with the largest  $T_{EDR}$  corresponding to the largest  $J$  for fixed  $T_{KMS}$ , and the smallest  $T_{EDR}$  corresponding to the smallest  $J$ . This is clearly evident in Figure 5. We have also verified that this effect is also present for

(a)  $\Omega\sigma = 1$ (a)  $\Omega\sigma = 1/100$ FIG. 5: EDR temperature for a black hole of mass  $M = 1/1000$ . The results are similar for  $\Omega\sigma = 1/100$ .

The insets show the EDR temperature for our first three values of the angular momentum, plotted on a linear scale (rather than a log scale, as is the case for the main plots).

Neumann and transparent boundary conditions, though the ‘crossover’ occurs at larger KMS temperatures than the Dirichlet case.

By comparing Figures 2-5, we see that there is no range of  $T_{KMS}$  for which the strong anti-Hawking effect overlaps with the weak anti-Hawking effect, with the weak anti-Hawking effect appearing for  $T_{KMS}\ell \gtrsim 1$ , while the strong anti-Hawking effect appears for  $T_{KMS}\ell \lesssim 0.1 - 0.5$ . The exact temperature range is dependent on the boundary conditions, energy gap, and in the case of the strong anti-Hawking effect, the angular momentum. Furthermore, the critical KMS temperature at which the strong anti-Hawking effect disappears becomes smaller for larger angular momentum, in contrast to the weak anti-Hawking effect where the critical temperature at which this effect appears has minimal dependence on angular momentum. In addition, we again note that the location of this critical temperature for the strong effect is highly dependent on the boundary conditions.

(a)  $\Omega\sigma = 1$ (a)  $\Omega\sigma = 1/100$ FIG. 6: Strong anti-Hawking effect for a near-extremal black hole of mass  $M = 1/1000$  and Dirichlet boundary conditions. The results are similar for  $\Omega\sigma = 1/10$ .

Our last consideration is that of the impact of changing the AdS length on the strong effect. Here the situation differs from the weak anti-Hawking effect as now there is a second length scale present ( $\sigma$ , the width of the switching function). In Figure 7, we consider the effect of changing the AdS length for a non-rotating BTZ black hole, compared to a near-extremal BTZ black hole. In the non-rotating case, increasing AdS length increases the range of  $T_{KMS}$  temperatures where the strong anti-Hawking effect holds. However, the marginal effect of increasing  $\ell$  is reduced for larger and larger values of the AdS length. We also see that for small  $T_{KMS}\ell$ , a larger AdS length will broaden the initial peak. In the case of a near-extremal black hole, the situation is similar. As we saw in Figure 4a, there was a tiny strong anti-Hawking effect present for near-extremal black holes. For larger AdS lengths, we similarly see that the temperature range of the strong anti-Hawking effect increases in size. However, we note that this effect is still relatively weak and only becomes noticeable for larger values of  $\ell$ .

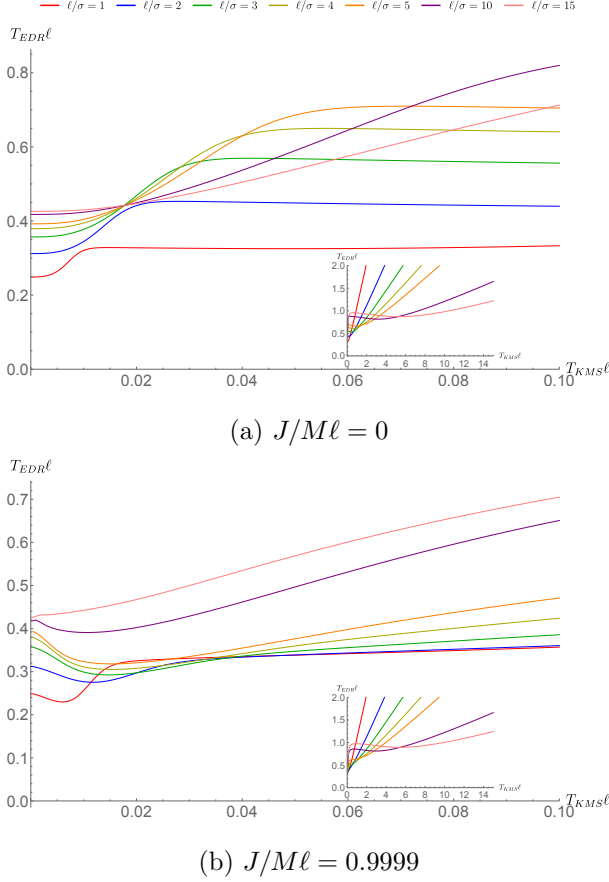


FIG. 7: Changing AdS lengths for the strong anti-Hawking effect for a black hole of mass  $M = 1/1000$ , Dirichlet boundary conditions, and energy gap of  $\Omega\sigma = 1/10$ . We plot KMS temperature down to  $T_{KMS}\ell = 10^{-5}$ . The insets show the effect of changing AdS length on the EDR temperature for larger values of  $T_{KMS}$ .

## CONCLUSION

As with entanglement harvesting [40], rotation can have a significant impact on the anti-Hawking effect. For large-mass black holes with Dirichlet and transparent boundary conditions, the weak anti-Hawking effect vanishes, as expected; it is present for Neumann boundary conditions [30]. In all cases the effects of rotation are negligible. But as the mass of the black hole decreases, rotation significantly amplifies the weak version of the effect.

The impact of rotation on the strong effect is somewhat inverted. We find that rotation tends to weaken the strength of the strong anti-Hawking effect for transparent and Neumann boundary conditions, with it nearly vanishing for near-extremal black holes. In contrast, for Dirichlet boundary conditions, larger angular momenta causes the strong anti-Hawking effect to be reduced before being amplified again.

Furthermore, for the strong anti-Hawking effect, the relationship between angular momentum and detector temperature is non-monotonic for each boundary condition, leading to a ‘crossover’ phenomenon that is most prominent for Dirichlet boundary conditions. For small  $T_{KMS}L$ , larger angular momenta yield smaller  $T_{EDR}L$ , whereas for larger values of  $T_{KMS}L$ , larger angular momenta yield larger  $T_{EDR}$ . More work is needed to better understand how this cross-over effect comes about and its dependence on the boundary conditions. It would also be interesting to consider whether 3+1 dimensional rotating black holes also exhibit these same findings as the rotating BTZ black hole.

While the weak anti-Hawking effect is independent of the AdS length  $\ell$ , increasing AdS length increases the range of  $T_{KMS}$  temperatures where the strong anti-Hawking effect holds. A larger AdS length will also broaden the initial peak for small  $T_{KMS}\ell$ . However as  $\ell$  continues to increase, its impact on the strong effect becomes increasingly marginal.

In summary, our results indicate that the effects of spacetime dragging on the quantum vacuum can significantly modify detector response as small field KMS field temperatures, as exemplified by the anti-Hawking effect(s). The role of boundary conditions is very important; indeed, it is surprising that there is such a strong dependence of the strong anti-Hawking effect on boundary conditions for small-mass rotating black holes. The origin of this effect merits further study.

*Acknowledgements* MR was funded by an Ontario Graduate Scholarship. This research was supported in part by the Natural Sciences and Engineering Research Council of Canada, Asian Office of Aerospace Research & Development Grant FA2386-19-1-4077, and the Perimeter Institute for Theoretical Physics. Research at Perimeter Institute is supported in part by the Government of Canada through the Department of Innovation, Science and Economic Development Canada and by the Province of Ontario through the Ministry of Colleges and Universities.

- 
- [1] Eduardo Martín-Martínez, Miguel Montero, and Marco del Rey. Wavepacket detection with the Unruh-DeWitt model. *Phys. Rev. D*, 87(6):064038, 2013.
  - [2] Nicholas Funai. *Investigations into quantum light-matter interactions, their approximations and applications*. PhD thesis, U. Waterloo (main), 2021.
  - [3] Eduardo Martín-Martínez, Alexander R. H. Smith, and Daniel R. Terno. Spacetime structure and vacuum entanglement. *Phys. Rev. D*, 93:044001, Feb 2016.
  - [4] Keith K. Ng, Robert B. Mann, and Eduardo Martín-Martínez. Over the horizon: Distinguishing the schwarzschild spacetime and the  $\mathbb{R}^3$  spacetime using an unruh-dewitt detector. *Phys. Rev. D*, 96:085004, Oct 2017.



- [5] Laura J Henderson, Robie A Hennigar, Robert B Mann, Alexander R H Smith, and Jialin Zhang. Harvesting entanglement from the black hole vacuum. *Classical and Quantum Gravity*, 35(21):21LT02, oct 2018.
- [6] Erickson Tjoa and Robert B. Mann. Harvesting correlations in schwarzschild and collapsing shell spacetimes. *Journal of High Energy Physics*, 2020(8):155, 2020.
- [7] Greg Ver Steeg and Nicolas C. Menicucci. Entangling power of an expanding universe. *Phys. Rev. D*, 79(4):044027, February 2009.
- [8] Zhiming Huang and Zehua Tian. Dynamics of quantum entanglement in de sitter spacetime and thermal minkowski spacetime. *Nuclear Physics B*, 923:458–474, 2017.
- [9] Stephen A. Fulling. Nonuniqueness of Canonical Field Quantization in Riemannian Space-Time. *Phys. Rev. D*, 7(10):2850–2862, May 1973.
- [10] P. C. W. Davies. Scalar production in Schwarzschild and Rindler metrics. *Journal of Physics A Mathematical General*, 8(4):609–616, April 1975.
- [11] W. G. Unruh. Notes on black-hole evaporation. *Phys. Rev. D*, 14(4):870–892, August 1976.
- [12] Geoffrey L Sewell. Quantum fields on manifolds: Pct and gravitationally induced thermal states. *Annals of Physics*, 141(2):201–224, 1982.
- [13] Ryogo Kubo. Statistical-mechanical theory of irreversible processes. i. general theory and simple applications to magnetic and conduction problems. *Journal of the Physical Society of Japan*, 12(6):570–586, 1957.
- [14] Paul C. Martin and Julian Schwinger. Theory of many-particle systems. i. *Phys. Rev.*, 115:1342–1373, Sep 1959.
- [15] R. Haag, N. M. Hugenholtz, and M. Winnink. On the equilibrium states in quantum statistical mechanics. *Communications in Mathematical Physics*, 5(3):215–236, 1967.
- [16] J. S. Bell and J. M. Leinaas. The Unruh Effect and Quantum Fluctuations of Electrons in Storage Rings. *Nucl. Phys. B*, 284:488, 1987.
- [17] I. Costa. SEPARABLE COORDINATES AND PARTICLE CREATION. 1. THE KLEIN-GORDON EQUATION. *Rev. Bras. Fis.*, 17:585–600, 1987.
- [18] Umberto Percoco and Victor M. Villalba. Particle creation in an asymptotically uniformly accelerated frame. *Class. Quant. Grav.*, 9:307–316, 1992.
- [19] Victor M. Villalba and Juan Mateu. Vacuum effects in an asymptotically uniformly accelerated frame with a constant magnetic field. *Phys. Rev. D*, 61:025007, 2000.
- [20] David C. M. Ostapchuk, Shih-Yuin Lin, Robert B. Mann, and B. L. Hu. Entanglement Dynamics between Inertial and Non-uniformly Accelerated Detectors. *JHEP*, 07:072, 2012.
- [21] B. L. Hu, Shih-Yuin Lin, and Jorma Louko. Relativistic Quantum Information in Detectors-Field Interactions. *Class. Quant. Grav.*, 29:224005, 2012.
- [22] Jason Doukas, Shih-Yuin Lin, B. L. Hu, and Robert B. Mann. Unruh effect under non-equilibrium conditions: oscillatory motion of an unruh-dewitt detector. *Journal of High Energy Physics*, 2013(11):119, 2013.
- [23] W.G. Brenna, Robert B. Mann, and Eduardo Martín-Martínez. Anti-unruh phenomena. *Physics Letters B*, 757:307–311, 2016.
- [24] Luis J. Garay, Eduardo Martín-Martínez, and José de Ramón. Thermalization of particle detectors: The unruh effect and its reverse. *Phys. Rev. D*, 94:104048, Nov 2016.
- [25] N. D. Birrell and P. C. W. Davies. *Quantum Fields in Curved Space*. Cambridge Monographs on Mathematical Physics. Cambridge University Press, 1982.
- [26] Lee Hodgkinson and Jorma Louko. Static, stationary, and inertial unruh-dewitt detectors on the btz black hole. *Phys. Rev. D*, 86:064031, Sep 2012.
- [27] Alexander R. H. Smith and Robert B. Mann. Looking inside a black hole. *Classical and Quantum Gravity*, 31(8):082001, April 2014.
- [28] Lee Hodgkinson, Jorma Louko, and Adrian C. Ottewill. Static detectors and circular-geodesic detectors on the Schwarzschild black hole. *Phys. Rev. D*, 89(10):104002, 2014.
- [29] Keith K. Ng, Lee Hodgkinson, Jorma Louko, Robert B. Mann, and Eduardo Martín-Martínez. Unruh-DeWitt detector response along static and circular geodesic trajectories for Schwarzschild-AdS black holes. *Phys. Rev. D*, 90(6):064003, 2014.
- [30] Laura J. Henderson, Robie A. Hennigar, Robert B. Mann, Alexander R. H. Smith, and Jialin Zhang. Anti-Hawking phenomena. *Phys. Lett. B*, 809:135732, 2020.
- [31] Lissa De Souza Campos and Claudio Dappiaggi. The anti-Hawking effect on a BTZ black hole with Robin boundary conditions. *Phys. Lett. B*, 816:136198, 2021.
- [32] Lissa de Souza Campos and Claudio Dappiaggi. Ground and thermal states for the Klein-Gordon field on a massless hyperbolic black hole with applications to the anti-Hawking effect. *Phys. Rev. D*, 103(2):025021, 2021.
- [33] Elizabeth Winstanley. Classical super-radiance in kerr-newman-anti-de sitter black holes. *Physical Review D*, 64(10), Oct 2001.
- [34] Marc Casals, Sam Dolan, Panagioti Kanti, and Elizabeth Winstanley. Bulk emission of scalars by a rotating black hole. *Journal of High Energy Physics*, 2008(06):071–071, Jun 2008.
- [35] Adrian C. Ottewill and Elizabeth Winstanley. Divergence of a quantum thermal state on Kerr space-time. *Phys. Lett. A*, 273:149–152, 2000.
- [36] Robert B. Mann and Sergei N. Solodukhin. Quantum scalar field on three-dimensional (BTZ) black hole instanton: Heat kernel, effective action and thermodynamics. *Phys. Rev. D*, 55:3622–3632, 1997.
- [37] Dharm Veer Singh and Sanjay Siwach. Scalar Fields in BTZ Black Hole Spacetime and Entanglement Entropy. *Class. Quant. Grav.*, 30:235034, 2013.
- [38] Francesco Bussola, Claudio Dappiaggi, Hugo R. C. Ferreira, and Igor Khavkine. Ground state for a massive scalar field in the BTZ spacetime with Robin boundary conditions. *Phys. Rev. D*, 96(10):105016, 2017.
- [39] I. Ablu Meitei, T. Ibungochouba Singh, S. Gayatri Devi, N. Premeshwari Devi, and K. Yugindro Singh. Quantum gravity effects on scalar particle tunneling from rotating BTZ black hole. *Int. J. Mod. Phys. A*, 33(12):1850070, 2018.
- [40] Matthew P. G. Robbins, Laura J. Henderson, and Robert B. Mann. Entanglement Amplification from Rotating Black Holes. *arXiv e-prints*, page arXiv:2010.14517, October 2020.
- [41] Smith, Alexander R. H. Detectors, reference frames, and time, 2017.
- [42] Christopher J. Fewster, Benito A. Juárez-Aubry, and Jorma Louko. Waiting for Unruh. *Classical and Quantum Gravity*, 33(16):165003, August 2016.
- [43] Maximo Banados, Claudio Teitelboim, and Jorge Zanelli. Black hole in three-dimensional spacetime.

- Physical Review Letters*, 69(13):1849–1851, September 1992.
- [44] Gilad Lifschytz and Miguel Ortiz. Scalar field quantization on the (2+1)-dimensional black hole background. *Phys. Rev. D*, 49:1929–1943, Feb 1994.
- [45] Steven Carlip. *Quantum Gravity in 2 + 1 Dimensions*. Cambridge Monographs on Mathematical Physics. Cambridge University Press, 1998.
- [46] Elias C. Vagenas. Two-Dimensional Dilatonic Black Holes and Hawking Radiation. *Modern Physics Letters A*, 17(10):609–618, January 2002.